OPAL PN 310
14 August 1997

Study of the running of α_s between LEP1 and LEP2

The OPAL Collaboration

Abstract

Using hadronic final states of e^+e^- annihilation events at LEP at centre-of-mass energies of $\sqrt{s} = M_{Z^0}, 130 - -136, 161$ and 172 GeV, we study effects of the running of α_s as predicted by QCD. Moments of the distributions of the event shape observables thrust and C parameter are compared to the expectations of $\mathcal{O}(\alpha_s^2)$ QCD. The higher moments of event shape observables are studied for the first time. The hadronisation corrections for these event shape moments are parametrised by power corrections. The evolution of jet production rates, mean jet multiplicity and event shape moments with $\sqrt{s}$ is determined. Our observations confirm the running of α_s as predicted by QCD. A model with constant α_s can be excluded with at least 95% confidence level.

This note describes preliminary OPAL results and is intended primarily for members of the collaboration.

1 Introduction

With the centre-of-mass (cms) energies explored by LEP1 and LEP2 the dependence of e^+e^- annihilation processes on $\sqrt{s}$ may be studied in identical experimental conditions. The analyses of the hadronic event samples at the various cms energies are expected to have similar systematic uncertainties.

The coupling constant $\alpha_s(Q)$ of the theory of strong interactions, Quantum Chromo Dynamics (QCD), is expected to depend on the energy scale Q of the process. In e^+e^- annihilation the scale Q is commonly identified with the cms energy, i.e. $Q = \sqrt{s}$. This so-called running of the strong coupling constant is a property fundamental to all renormalisable gauge theories. It is a particular feature of QCD that the effects of the running coupling are comparatively large, mainly because the value of the coupling is large. QCD is thus an example of a gauge theory which is well suited for tests of the running behaviour of the couplings in gauge theories in general. Summaries of experimental tests may be found e.g. in [1, 2].

In previous publications we have measured the strong coupling α_s with e^+e^- annihilation data at LEP1 ($\sqrt{s} = 91.2$, corresponding to the Z^0 peak), at LEP1.5 ($\sqrt{s} = 130$ and 136 GeV) and at LEP2 ($\sqrt{s} = 161$ and 172 GeV) [3–7]. Comparing this data with a running value of α_s the χ^2 probability is around 30% for a consistent set of observables: the thrust $1 - T$, the heavy jet mass M_H and the total and wide jet broadening, B_T and B_W. In order to demonstrate the experimental significance of the observed energy dependence we compare this result with the hypothesis that α_s is constant. For α_s constant the χ^2 probability is less than 1%. Since both LEP2 results were below expectation from QCD the confidence level for excluding a constant α_s may be too optimistic. It is the aim of this note to analyse all data consistently, with different observables, in order to test the compatibility of the data with a running α_s, as predicted by QCD, or a constant α_s. The high statistics data sample available at LEP1 energies provides an accurate determination of our observables, whereas the smaller data samples at LEP1.5 and LEP2 are effectively used to test the changes induced by the running of α_s.

In order to make optimal use of the limited statistics which is presently available at the high energy points we concentrate on inclusive quantities, i.e. those where the entire event sample is used. These are the mean jet multiplicity $\langle N_{\rm jet} \rangle$, based on the Durham jet finding algorithm [8], as a function of the jet resolution parameter $y_{\rm cut}$, and the first three moments of the distributions of the event shape observables thrust, $1 - T$, and the C-parameter, C [3, 5]. These observables are different from the ones used in our earlier publications where we fitted limited ranges of differential distributions in order to measure α_s. In addition the moments of the event shape observables allow the use of power corrections instead of Monte Carlo hadronisation corrections.

In section 2 the theoretical calculations which are needed are summarised. In section 3 the OPAL detector is briefly described. In section 4 the analysis is described while in section 5 the results are presented. In section 6 a summary is given.

2 Calculations

2.1 Running of α_s

The running of the strong coupling α_s is described by the renormalisation group equation which states that results from a gauge theory should not depend on the energy scale at which the theory is renormalised. From this requirement one obtains a differential equation for the energy dependence of the strong coupling:

$$\mu^2 \frac{\partial \alpha_s(\mu)}{\partial \mu^2} = \beta(\alpha_s(\mu)) \quad . \tag{1}$$

Here μ is the energy at which the coupling is evaluated and $\beta(\alpha_s(\mu)) = \beta_0\alpha_s^2(\mu)+\beta_1\alpha_s^3(\mu)+\beta_2\alpha_s^4(\mu)+\mathcal{O}(\alpha_s^5)$ is the β-function of QCD calculated at the three-loop level (see e.g. [9]). The first order coefficient is $\beta_0 = (33-2\mathrm{n_f})/(12\pi)$ where $\mathrm{n_f} = 5$ is the number of active quark flavours. To first order the running of α_s may be written as

$$\frac{\alpha_s(Q)}{\alpha_s(\mu)} = 1 + 2\beta_0\alpha_s(Q)\ln(x_\mu) \quad , \tag{2}$$

where $x_\mu = \mu/Q$ is the renormalisation scale parameter given by the ratio of the energy μ to which the strong coupling is run and the energy Q at which the strong coupling is defined. It is seen that the running is logarithmic, i.e. a step in energy from e.g. 10 GeV to 20 GeV is comparable to a step from 100 GeV to 200 GeV. However, the effect of the running also depends on the actual value of $\alpha_s(Q)$. Therefore one expects the size of the effect to be smaller at higher energies since with increasing energy the value of $\alpha_s(Q)$ decreases.

2.2 Fixed Order Predictions

The moments of event shape observables, $\langle y^n \rangle = 1/\sigma \int dy\, y^n d\sigma/dy$, and the mean jet multiplicity $\langle N_{\mathrm{jet}} \rangle$ as a function of y_{cut}, are predicted in $\mathcal{O}(\alpha_s^2)$ as a function $F^{pert}(\alpha_s, x_\mu)$ (see e.g. [10]):

$$F^{pert} = \frac{\alpha_s(x_\mu Q)}{2\pi} A + \left(\frac{\alpha_s(x_\mu Q)}{2\pi}\right)^2 (B - A(4\pi\beta_0 \ln(x_\mu) - 2)) \quad . \tag{3}$$

The coefficients A and B are calculated for each observable using the QCD matrix element integration program EVENT2 [11]. We include the energy dependence explicitly in relation (3) to emphasise that in perturbative QCD any cms energy dependence stems directly from the running of the strong coupling α_s. The renormalisation scale dependent term $4\pi\beta_0 \ln(x_\mu)$ in equation (3) stems also from introducing a running α_s into the perturbative prediction.

For the moments of some event shape observables a treatment of non-perturbative effects is possible by estimating their power corrections. These calculations replace non-perturbative hadronisation corrections which are based on Monte Carlo models. In the

case of $1-T$ and C the non-perturbative contribution F_n^{pow} to the moment n can be written as [12, 13]:

$$F_n^{pow} = a_f \frac{1}{n^2} \left(\frac{\mu_I}{Q}\right)^n \left(\bar{\alpha}_{n-1}(\mu_I) - \alpha_s(Q) - \frac{\beta_0}{2\pi}\alpha_s(Q)^2 \left(\ln\left(\frac{Q}{\mu_I}\right) + \frac{K}{\beta_0} + \frac{1}{n}\right)\right) \quad . \qquad (4)$$

In this equation μ_I is the so-called infrared matching scale at which the perturbative and non-perturbative calculations are matched and $\bar{\alpha}_{n-1}(\mu_I)$ is a free parameter for each moment. Both μ_I and $\bar{\alpha}_{n-1}(\mu_I)$ are independent of the observable y. The terms K and a_f are $K = (\frac{67}{18} - \frac{\pi^2}{6})\mathrm{C_A} - \frac{5}{9}\mathrm{n_f}$ and $a_f = \frac{4\mathrm{C_F}}{\pi}$ or $a_f = 6\mathrm{C_F}$ for the moments of $1-T$ and C, respectively. The constants $\mathrm{C_F} = 4/3$ and $\mathrm{C_A} = 3$ are the QCD colour factors. The infrared matching scale is usually taken in the range 1 GeV$< \mu_I <$ 3 GeV [12].

The complete prediction for the moment n of the event shape observable y is then the combination of equations (3) and (4):

$$\langle y^n \rangle = F_n^{pert} + F_n^{pow} \quad , \qquad (5)$$

where the index n ($n = 1, 2, 3$) refers to the order of the moment. Note that, as a modification, in equation (4) we use the scale Q, independent of x_μ, because in principle we expect the power corrections to be independent of missing higher orders in the perturbative prediction, equation (3). In practice higher order contributions are partly absorbed by the power corrections leading to correlations between α_s, x_μ and the non-perturbative parameters $\bar{\alpha}_{n-1}$.

Already at LEP1 the power corrections of the second and third moment of $1-T$ and C are suppressed by factors of $(\mu_I/Q)^2 \simeq 5 \cdot 10^{-4}$ and $(\mu_I/Q)^3 \simeq 1 \cdot 10^{-5}$ for $\mu_I = 2$ GeV for all observables [12]. There is no data available for higher moments at lower energies to test this prediction. Instead we generated 10 000 Monte Carlo events each at $Q = 14$, 22, 35, 44, 55, 91.173, 133, 161, 172 and 205 GeV with the JETSET 7.4 [14] and the HERWIG 5.9 [15] Monte Carlo programs[1] without initial state radiation (ISR) at the hadron level (see below in section 4.1 for a precise definition of hadron level). The first three moments of $1-T$ and C were computed at each energy and the energy evolution of each moment was fitted by equation (5) with $x_\mu = 0.05$ kept fixed and $\mu_I = 2.0$ GeV. A low value of the renormalisation scale parameter is necessary to obtain consistent values of α_s with the higher moments. Fits to two or three moments at fixed energy also prefer low values of x_μ. For completeness the results for $1-T$ and C are given in table 1 and are shown for JETSET in figure 1.

One can clearly see that the full prediction (full lines) and the purely perturbative predictions (dashed lines) merge at smaller values of Q for higher moments due to the stronger suppression of non-perturbative effects in the higher moments. The overall description of the Monte Carlo simulation by the theory is reasonable. The values for $\alpha_s(M_{\mathrm{Z^0}})$ are consistent with each other within 5% for JETSET and 10% for HERWIG. For some fits we obtain large values of χ^2/d.o.f. dominated by the low energy points. The non-perturbative parameters $\bar{\alpha}_{n-1}$ are also consistent with each other except for $\bar{\alpha}_2$, which

[1] The parameter sets of these Monte Carlo programs are documented in [16]. The Monte Carlo programs simulate the cms energy dependence of the first moment of $1-T$ reasonably well [6]. The HERWIG parameter `CLMAX` has been changed to 3.75 for HERWIG 5.9.

differs significantly between $1-T$ and C. This might be due to other non-perturbative effects not described by the power corrections which are important at lower energies. However, this will not affect the analysis since we have data at high energy only, where the power corrections are strongly suppressed.

2.3 Resummed Prediction for $\langle N_{\rm jet}\rangle$

For the mean jet multiplicity, $\langle N_{\rm jet}\rangle$, power correction terms are not yet available. However, besides the second order calculation of the form given in equation (3), resummation of terms containing large logarithms which arise from soft and collinear singularities has been performed [17]. For small values of $y_{\rm cut}$ the effective expansion parameter is not simply α_s, but becomes $\alpha_s \ln^2(y_{\rm cut})$ (leading logarithm). NLLA QCD calculations sum these terms, including subleading logarithms, to all orders in α_s.

The calculation of $\langle N_{\rm jet}\rangle$ can be written in the form [17] (where $\bar{\alpha_s} = \alpha_s/2\pi$):

$$\langle N_{\rm jet}\rangle = 2 + \sum_{n=1}^{\infty} \mathcal{H}_n \, \bar{\alpha_s}^n \qquad \text{with} \qquad \mathcal{H}_n = \sum_{m=0}^{2n} H_{nm} \ln^m(y_{\rm cut}). \tag{6}$$

The $\mathcal{O}(\alpha_s^2)$ calculations of equation (3) sum the terms in m for $n=1$ and $n=2$. The NLLA predictions resum all terms n for $m=2n$ (leading logarithms) and $m=2n-1$ (sub-leading logarithms). H_{nm} is the coefficient for powers of α_s and $\ln(y_{\rm cut})$ of n and m, respectively.

At LEP the $\mathcal{O}(\alpha_s^2)$ calculations provide an accurate description of $\langle N_{\rm jet}\rangle$ at large values of $y_{\rm cut}$, near the kinematic limit, where the logarithmic contributions are small. On the other hand, the NLLA prescription is accurate at very small values of $y_{\rm cut}$, where the logarithmic terms are dominant and contributions of $\mathcal{O}(y_{\rm cut})$ (contributions with $m < 2n-1$) can be neglected. By using $y_{\rm cut}$ as a 'sliding' scale, $\langle N_{\rm jet}\rangle$ probes the range of validity of these approximations. As a consequence we find that determination of α_s is biased towards large values using the $\mathcal{O}(\alpha_s^2)$ calculations at small values of $y_{\rm cut}$ or using the NLLA calculations at large values of $y_{\rm cut}$ for a fixed renormalisation scale $x_\mu = 1$.

To utilise the full results of these calculations, various matching schemes between the $\mathcal{O}(\alpha_s^2)$ and the NLLA calculations are available [4]. The matching schemes differ in higher orders. In the R matching scheme the $\mathcal{O}(\alpha_s)$ and $\mathcal{O}(\alpha_s^2)$ terms of the NLLA calculation are subtracted and replaced by the corresponding exact $\mathcal{O}(\alpha_s^2)$ terms:

$$\langle N_{\rm jet}\rangle = \langle N_{\rm jet}\rangle_{NLLA} - \mathcal{H}_1\bar{\alpha_s} - \mathcal{H}_2\bar{\alpha_s}^2 + A(y)\bar{\alpha_s} + [B(y) - 2A(y)]\,\bar{\alpha_s}^2 \quad , \tag{7}$$

whereas in the procedure analogous to the $\ln(R)$ matching one calculates $\langle N_{\rm jet}\rangle$ as:

$$\begin{aligned} \langle N_{\rm jet}\rangle \;\; = \;\; & 1 + [\langle N_{\rm jet}\rangle_{NLLA} - 1] \exp\left\{ -\mathcal{H}_1\bar{\alpha_s} - \left[\mathcal{H}_2 - \tfrac{1}{2}\mathcal{H}_1^2\right]\bar{\alpha_s}^2 \right. \\ & \left. + A(y)\bar{\alpha_s} + \left[B(y) - \tfrac{1}{2}A(y)^2\right]\bar{\alpha_s}^2 \right\} \quad . \end{aligned} \tag{8}$$

The coefficients H_{12}, H_{11}, H_{24} and H_{23} are given in equation (8) of [17]. In this analysis we also consider a variant of the $\ln(R)$ matching scheme, in which those terms are added explicitly to the NLLA calculation that are proportional to $\mathcal{O}(\alpha_s^2)$ but which were not considered in the NLLA approximation, i.e. H_{22} and H_{21}. The values of these terms were determined from fitting the coefficient $B(y)$ at very small values of $y_{\rm cut}$, where terms proportional to $\mathcal{O}(y_{\rm cut})$ can be neglected.

3 The OPAL detector

The OPAL detector is described in detail in [18]. The analysis presented here relies mainly on the reconstruction of charged particles in the tracking chambers and of energy deposits (clusters) in the electromagnetic calorimeters.

All tracking systems are located inside a solenoidal magnet which provides a uniform axial magnetic field of 0.435 T along the beam axis[2]. The magnet is surrounded by a lead glass electromagnetic calorimeter and a hadron calorimeter of the sampling type. Outside the hadron calorimeter, the detector is surrounded by a system of muon chambers. There are similar layers of detectors in the endcap regions.

The main tracking detector is the central jet chamber. This device is approximately 4 m long and has an outer radius of about 1.85 m. It has 24 sectors with radial planes of 159 sense wires spaced by 1 cm. The momenta of tracks are measured, with a precision of the component in the x-y plane, p_T, parametrised by $\sigma_{p_T}/p_T = \sqrt{0.02^2 + (0.0015 \cdot p_T[\mathrm{GeV}/c])^2}$. The electromagnetic calorimeters in the barrel and the endcap sections of the detector consist of a total of 11 704 lead glass blocks with a depth of 24.6 radiation lengths in the barrel and more than 22 radiation lengths in the endcap regions.

4 Data Analysis

4.1 LEP1 Data

The determination of the jet production rates and the first three moments of the $1 - T$ and C distributions for the LEP1 data proceeds as follows. The main results are based on a data sample of about 1.7 million hadronic Z^0 decays collected in 1994. To preselect hadronic decays of the Z^0 the criteria given in [19] are applied. We define as particles both tracks recorded in the tracking chambers, with transverse momentum $p_T > 150$ MeV/c, and clusters recorded in the electromagnetic calorimeter, with a minimum energy of 100 MeV in the barrel and 250 MeV in the endcap sections [5]. We require the event to have more than six well reconstructed tracks and the angle of the thrust axis with the beam direction to fulfil $|\cos\theta_T| < 0.9$. The dominant background from e^+e^- annihilations into $\tau^+\tau^-$ and two-photon events is estimated to be less than 1%.

The correction of event shape moments and jet production rates for the effects of limited resolution of the detector and the acceptance of the selection cuts is performed using Monte Carlo event samples with full simulation of the OPAL detector [20]. The results from the simulated events passed through the same analysis procedure as the data are referred to as being at the *detector level*. The results from simulated events without detector simulation or ISR and with all particles with lifetimes greater than $3 \cdot 10^{-10}$ s declared stable are called at the *hadron level*. For future reference we also introduce the *parton level* where the results are based on the remaining quarks and gluons after termination of the Monte Carlo parton shower. The ratio of results obtained at the

[2]In the OPAL coordinate system the x axis points towards the centre of the LEP ring, the y axis points upwards and the z axis points in the direction of the electron beam. The polar angle θ and the azimuthal angle ϕ are defined with respect to z and x, respectively, while r is the distance from the z-axis.

hadron level to results obtained at the detector level defines the correction factors which we apply to the data. Our standard corrections are based on the JETSET 7.4 Monte Carlo.

As systematic variations of the analysis we use detector corrections derived from the HERWIG 5.9 Monte Carlo, we use a special algorithm, MT, to avoid double counting the energy of charged particles in the clusters in the electromagnetic calorimeter [21], we tighten the cut on $\cos\theta_T$ to $|\cos\theta_T| < 0.7$ and we use the combined on-peak data from 1993 and 1995 rather than the 1994 data.

For $\langle N_{\rm jet}\rangle$ instead of using MT we repeat the analysis using tracks only and clusters only as alternatives to the main result based on all tracks and clusters. The maximum difference between these three results, divided by $\sqrt{12}$, is taken as this systematic uncertainty, because we expect the true value to be within the range defined by these three results. The differences relative to the standard results are added in quadrature to define the total experimental systematic error. The total experimental uncertainties are dominated by the effects of using the HERWIG-based detector corrections.

4.2 LEP1.5 and LEP2 Data

From the high energy data samples we determine the jet production rates and the first three moments of the $1-T$ and C distributions. The analysis of the high energy data follows as closely as possible our previous publications [5–7]. We apply the same preselection of hadronic events [19] and use the same requirements to select well reconstructed tracks and clusters [5]. We demand that the events have more than six well reconstructed tracks and that the angle of the thrust axis with the beam direction satisfies $|\cos\theta_T| < 0.9$.

Hadronic decays of a virtual intermediate s-channel Z^0 or γ at energies close to the cms energy, i.e. with only small losses due to ISR, so called *non-radiative events*, are selected by requiring the reconstructed invariant mass of the hadronic system $\sqrt{s'}$ [7] to be within 10 GeV of the nominal cms energy $\sqrt{s}$: $\sqrt{s} - \sqrt{s'} < 10$ GeV. As an alternative selection we apply the cuts given in [5] which employ the correlation between missing energy and momentum in the event and also the energy of energetic ISR photon candidates in the electromagnetic calorimeter. At $\sqrt{s} = 172$ GeV we reduce the additional background from non-QCD final states where four fermions come from the electroweak vertex (4-fermion final states). This is achieved by applying a cut on the probability that after reconstructing four jets the event configuration is consistent with coming from a second-order QCD process [7]. This background is dominated by the production of W^+W^- pairs with the subsequent decay of both W bosons into hadrons. The resulting event samples are expected to contain about 6% events involving ISR of more than 10 GeV at all high energy points and about 7% 4-fermion final states at 161 and 172 GeV.

The remaining background from 4-fermion final states is subtracted based on simulated events from the grc4f Monte Carlo event generator [22] before detector corrections are applied. The correction procedure for detector resolution and acceptance of cuts is the same as described in subsection 4.1. The standard correction factors are based on the PYTHIA 5.7 Monte Carlo [14] which includes a more complete treatment of ISR compared to JETSET 7.4.

We use the same systematic variations of the analyses as in our previous publica-

tions [5–7] and the method described in [6] to estimate the influence of statistical fluctuations on the systematic uncertainties throughout. For the LEP1.5 data we include an additional systematic check compared to those presented in [5], by using HERWIG 5.9 to determine the detector corrections. In this way, the treatment of the LEP1.5 data is made similar to the treatment of the LEP1 and LEP2 data.

5 Results

5.1 Moments of Event Shape Observables

5.1.1 Simultaneous Fits

In order to verify that $\mathcal{O}(\alpha_s^2)$ QCD is able to describe the data after the corrections for non-perturbative effects, we perform simultaneous fits of equation (5) to the first three moments at the four energy points, taking into account the experimental errors of each moment and the correlations between the moments as determined from the LEP1 data. The fits are based on the χ^2 method and α_s, $\bar{\alpha}_0$ and x_μ are varied at the same time. The correlations are employed to calculate a covariance matrix for the moments at each energy point, in order to calculate the χ^2 contribution of a given energy point.

The fits use $\mathcal{O}(\alpha_s^2)$ QCD, and power corrections for only the first moment. When x_μ is allowed to vary freely we find an adequate description of the first three moments of $1-T$ and C at each of the cms energy points. The fitted values of α_s and x_μ, as listed in table 2, are compatible with those obtained in analyses of the differential distributions of $1-T$ and C [3, 4]. The fits are shown in figures 2 a) to d) and 3 a) to d) as the full lines.

The simultaneous fits of all energy points also allow a determination of the non-perturbative parameter for the first moment, $\bar{\alpha}_0$. For $1-T$ we find $\bar{\alpha}_0 = 0.322 \pm 0.056$ and for C we find $\bar{\alpha}_0 = 0.249 \pm 0.020$ where the errors are experimental uncertainties. The parameters x_μ and $\bar{\alpha}_0$ are strongly correlated. The values for $\bar{\alpha}_0$ found in the fits with x_μ free are smaller than but consistent with other determinations [12, 23, 24]. There is also fairly good agreement with the corresponding values shown in table 1.

Allowing $\bar{\alpha}_1$ to vary leads to unstable fits with little improvement in χ^2/d.o.f. and large errors on $\bar{\alpha}_1$. We conclude that the fits have only small sensitivity to the non-perturbative parameter $\bar{\alpha}_1$ and it is thus taken to be zero. The non-perturbative parameter $\bar{\alpha}_2$, which is suppressed by another power of Q, is also taken to be zero.

Statistical uncertainties are estimated by a fit with statistical errors only. Experimental uncertainties are taken from the error returned by the fit. When the fits are performed for each of the systematic variations of the LEP1 analysis (see section 4.1) and the deviations relative to the standard result are added in quadrature we find an uncertainty consistent with the error returned by the fit.

Theoretical uncertainties are estimated as follows. The effect of missing higher order terms in the $\mathcal{O}(\alpha_s^2)$ truncated QCD prediction is evaluated by performing each fit twice, once with x_μ free (as described above) and once with fixed $x_\mu = 1.0$ [3, 4] and $\bar{\alpha}_0$ kept identical to the result from the fit with free x_μ. We performed the fits with $x_\mu = 1.0$ with and without the correlations between the moments. We found that for these fits we have to ignore the correlations in order to obtain stable results. To assure that the

result is equally distant to the two values of α_s obtained with $x_\mu = 1$ and with the fitted value for x_μ, the average of the two fit results defines our measurements of α_s; these are shown in table 2. The fits with $x_\mu = 1.0$ do not describe the data well, as was observed previously for differential distributions [3,4], but they are part of the established procedure to estimate the effects of missing higher orders in the $\mathcal{O}(\alpha_s^2)$ truncated QCD. The fits are also shown in figures 2 a) to d) and 3 a) to d) as the dashed lines. The renormalisation scale uncertainty is chosen to be the difference between the fit results with x_μ free and $x_\mu = 1.0$ kept fixed divided by $\sqrt{12}$, because the variation of x_μ covers a range which contains the true result with a large probability[3] [25].

The uncertainty due to the infrared matching scale μ_I is estimated by changing μ_I to 1 and 3 GeV, and by taking the larger deviation with respect to the standard result as the error. In order to test the sensitivity to the particular hadronisation model we are using, namely the power corrections, we perform a measurement where the hadronisation corrections to the data are made using multiplicative corrections derived from the JETSET 7.4 Monte Carlo. We fit equation (3) to the data and take the difference relative to the standard result as the uncertainty. The individual contributions are added in quadrature to define the total theoretical uncertainty.

The theoretical uncertainties are dominated by the variation of the renormalisation scale parameter x_μ. This observation and the central results we find are consistent with our previous analysis using $\mathcal{O}(\alpha_s^2)$ QCD and differential distributions of event shape observables [3, 4]. Since the effect of a variation of the renormalisation scale is proportional to the lowest order missing higher order term (i.e. $\mathcal{O}(\alpha_s^3)$) we conclude that effects of missing higher orders may also be large in $\mathcal{O}(\alpha_s^2)$ analyses of moments of event shape distributions. Theoretical uncertainties are correlated between the energy points and will therefore be of reduced influence on the test of the running of α_s.

5.1.2 Test of the Running of α_s

In order to test the running of α_s we perform fits of QCD with power corrections and a $\mathcal{O}(\alpha_s^3)$ running α_s and compare these to fits with power corrections and a constant α_s. We examine the values of χ^2/d.o.f. and the corresponding χ^2 probabilities to assess the consistency of these hypotheses with the data.

We perform separate fits to each moment using the four energy points. This is necessary, because we have to perform fits with a constant α_s with $x_\mu = 1$, i.e. the term $\approx \ln(x_\mu)$ in equation (3) vanishes, since for a truly constant α_s there should be no dependence on x_μ left in the theory. Simultaneous fits as presented above with a constant α_s and $x_\mu = 1$ result in large values of χ^2/d.o.f. due to the fact that a reasonable simultaneous fit of several moments at any given energy point is only possible for small values of x_μ. By performing separate fits for each moment the analysis is sensitive only to direct effects of the running of α_s as a function of $\sqrt{s}$.

In table 3 we list the values of $\alpha_s(M_{Z^0})$, χ^2/d.o.f. and the χ^2 probability P_{χ^2} from the separate fits to the first, second and third moments. The first row contains results obtained with the values of x_μ given in table 2 for $1 - T$ and C, while the second row

[3]This procedure differs somewhat from earlier publications [3,4] where we took half of the full range as the renormalisation scale uncertainty.

gives results for the same fits with $x_\mu = 1$. The third row presents the results of fits with a constant α_s, $x_\mu = 1$. In all three rows the value for $\bar{\alpha}_0$ is taken from table 2. The fourth row shows the results from fits with a constant α_s, without power corrections to the data. In this case the data are corrected for hadronisation effects using the JETSET 7.4 Monte Carlo. In figure 4 we show the fits corresponding to row one and row three of table 3. The solid lines represent the $\mathcal{O}(\alpha_s^2)$ fits including power corrections with a running α_s, and the dashed lines represent fits to constant α_s, with power corrections for the first moments. The perturbative part of the fits to the first moments with a running α_s is shown by the dotted lines.

The fits with a $\mathcal{O}(\alpha_s^3)$ running α_s are found to have values of χ^2/d.o.f. of about unity with corresponding χ^2 probabilities between 32% and 55%. This observation is independent of whether x_μ is fitted or fixed to $x_\mu = 1$. Consistent values of $\alpha_s(M_{Z^0})$ in the fits to the various moments are only obtained when the fitted value of x_μ from the corresponding simultaneous fit, as listed in table 2, is used.

The fits with constant α_s have significantly larger values of χ^2/d.o.f. in all cases. Due to the smaller statistical and experimental errors of the moments of C, we observe that the fits to the moments of C are more sensitive to effects of the running of α_s. The Monte Carlo hadronisation corrections exhibit a stronger cms energy dependence than the power corrections. Thus, the fits with Monte Carlo based hadronisation corrections and a constant α_s yield smaller values of χ^2/d.o.f. than the same fits with power corrections for both $1-T$ and C. This can be interpreted as a hadronisation model dependence of the tests of the running of α_s. Based on this information we conservatively choose the fit to the first moment of C with Monte Carlo based hadronisation corrections which results in a confidence limit of at least 95% for the exclusion of the model with a constant α_s between the LEP1 and LEP2 energy points.

5.2 Jet Production Rates

We also use the jet production rates, $R_{\rm n}(y_{\rm cut}) = \sigma_n(y_{\rm cut})/\sigma_{tot}$, to observe the effect of the running of α_s. The leading term for $R_{\rm n}(y_{\rm cut})$ in perturbative calculations is proportional to $\alpha_s^{\rm n-2}$ (for $n \geq 2$). Hence one expects an increase in the change of $R_{\rm n}(y_{\rm cut})$ between the LEP1 and LEP2 data as n becomes larger. The jet production rates for the LEP1.5 and LEP2 data with respect to LEP1 are seen from figure 5 to be consistent with this effect. In this figure we show $R_{\rm n}(y_{\rm cut})$ for the Durham scheme as a function of $y_{\rm cut}$, at the hadron level. The histogram shows the result from the LEP1 data for which the band represents the systematic uncertainty. The statistical uncertainty is much smaller than the systematic uncertainty. The points in the figure show the LEP1.5 and LEP2 data. The systematic uncertainties were calculated as described in section 4. Since there are only small differences between the jet rates at 161 and 172 GeV, because the change in cms energy is small, we added the data samples at 161 and 172 GeV to increase the statistical significance. We interpret the clearly visible effect as due to the running of α_s.

However, quantitative comparison to theoretical calculations is difficult since fixed order results are not available beyond $\mathcal{O}(\alpha_s^2)$. To this order, the four jet production rate goes to infinity for $y_{\rm cut} \to 0$, and the five jet rate is not defined. Resummed calculations exist [26] that take into account large logarithms of the type $\alpha_s \ln^2(y_{\rm cut})$, but they are

not matched to the $\mathcal{O}(\alpha_s^2)$ predictions and only describe the jet production rates at small values for $y_{\rm cut}$. In addition, hadronisation corrections become large for $y_{\rm cut}$ less than about 10^{-3}. We therefore do not use $R_{\rm n}(y_{\rm cut})$ but the mean jet multiplicity to study effects of the running of α_s.

5.3 Mean Jet Multiplicity

Calculations in $\mathcal{O}(\alpha_s^2)$ matched to NLLA resummations are available for $\langle N_{\rm jet}\rangle$, as described in section 2.3. This observable also has the experimental advantage of being fully inclusive, i.e. it utilises the full data statistics at each value of $y_{\rm cut}$ (which implies that $\langle N_{\rm jet}\rangle$ is correlated between points of different $y_{\rm cut}$). We study three values for $y_{\rm cut}$, $y_{\rm cut} = 0.001, 0.005$ and 0.04.

In figure 6 a) we show $\langle N_{\rm jet}\rangle - 2$ for data taken at $\sqrt{s} = M_{\rm Z^0}, 130 - -136, 161$ and 172 GeV, respectively, as a function of $y_{\rm cut}$, at the hadron level with statistical uncertainties. We choose to show $\langle N_{\rm jet}\rangle - 2$ since already $\langle N_{\rm jet}\rangle = 2$ at $\mathcal{O}(\alpha_s^0)$. The inset in the figure enlarges the region near the kinematic limit. The figure shows that $\langle N_{\rm jet}\rangle$ decreases as the energy increases, which is seen to be a larger effect at smaller values of $y_{\rm cut}$. For very small values of $y_{\rm cut}$, non-perturbative hadronisation effects are sizable and cms energy dependent. Hence part of the change in $\langle N_{\rm jet}\rangle$ as a function of $\sqrt{s}$ at very small values of $y_{\rm cut}$ may be explained by these non-perturbative effects. At $y_{\rm cut} = 0.001$, the Monte Carlo correction for hadronisation effects (the ratio between $\langle N_{\rm jet}\rangle - 2$ at the parton and hadron levels) is about 20% at $\sqrt{s} = M_{\rm Z^0}$, whereas for LEP2 this ratio is smaller than 5%.

For larger values of $y_{\rm cut}$, the decrease in $\langle N_{\rm jet}\rangle$ as a function of $\sqrt{s}$ is dominated by the running of α_s, and thus the running of α_s can be measured reliably in this region. For $y_{\rm cut}$ larger than about $y_{\rm cut} \sim 0.005$ the hadronisation corrections are approximately 5% for the different cms energy points.

To establish the running of α_s, we perform fits to all four cms energy points simultaneously for $y_{\rm cut} = 0.001$, 0.005 and 0.04. We fit data corrected to the parton level using multiplicative Monte Carlo correction factors. The fits are performed in the R-, the $\ln(R)$, and the modified $\ln(R)$ matching schemes, as described in section 2. We fit α_s with the renormalisation scale fixed to $x_\mu = 1$, because the inclusion of the NLLA terms reduces the need for small values of x_μ [4]. For $y_{\rm cut} = 0.04$, where 2- and 3-jet final states dominate, we fit in addition the pure $\mathcal{O}(\alpha_s^2)$ calculations, with x_μ fixed at $x_\mu = 1$ and $x_\mu = 0.067$. The latter value for x_μ was obtained as the best fit in [4] using the $\mathcal{O}(\alpha_s^2)$ fits to the data at $\sqrt{s} = M_{\rm Z^0}$ for the range $0.02 \leq y_{\rm cut} \leq 0.1$.

In figures 6 b), c) and d) we show the results of the fits for the three values of $y_{\rm cut}$ as a function of cms energy. The points show the data for $\langle N_{\rm jet}\rangle$ at the parton level. The systematic uncertainties are evaluated as described in section 4. The full lines are the results of the fits, with $\mathcal{O}(\alpha_s^3)$ QCD predictions of the running of α_s. The fits to the R-, the $\ln(R)$, the modified $\ln(R)$ matching schemes and the $\mathcal{O}(\alpha_s^2)$ predictions are indistinguishable in the figures.

The values we obtain for $\alpha_s(M_{\rm Z^0})$ are listed in table 4. We present the values for α_s as determined in the R-, the $\ln(R)$ and the modified $\ln(R)$ matching schemes and for $y_{\rm cut} = 0.04$ results for α_s using the $\mathcal{O}(\alpha_s^2)$ predictions as well. For $y_{\rm cut} = 0.005$ and

$y_{\rm cut} = 0.04$ the results for α_s for the R and the $\ln(R)$ matching schemes and also for the $\mathcal{O}(\alpha_s^2)$ calculations are consistent with the ones determined in our earlier publication [4]. The differences between matching schemes may be interpreted as theoretical uncertainties due to missing higher order terms.

For $y_{\rm cut} = 0.001$, a value of $y_{\rm cut}$ smaller than was used before in [4], our results for α_s are consistent with values we obtain at larger $y_{\rm cut}$ for each of the matching schemes. This implies that even at this low value of $y_{\rm cut}$ the data is well described by the calculations including hadronisation corrections. The values for χ^2/d.o.f. of all the fits are good, resulting in χ^2 probabilities P_{χ^2} ranging from 0.51 for $y_{\rm cut} = 0.001$ to 0.75 for $y_{\rm cut} = 0.04$. The χ^2/d.o.f. and the χ^2 probabilities P_{χ^2} are essentially identical for each of the matching schemes as well as for the pure $\mathcal{O}(\alpha_s^2)$ calculations and are therefore not given for each calculation separately.

In figure 6 the dashed lines show fits to the data with the value of α_s kept constant. It can clearly be seen that fits with constant α_s provide a worse description of the data than fits with running α_s, especially for the lowest value of $y_{\rm cut}$. This is quantified in table 4, where we list the χ^2/d.o.f. and the χ^2 probabilities P_{χ^2} for fixed values for α_s. The results we obtain for α_s for the various matching schemes and also for the $\mathcal{O}(\alpha_s^2)$ calculation, for a constant value of α_s, are similar to the ones quoted in the table 4 for a running α_s, and thus are not shown.

For small values of $y_{\rm cut}$ the probability P_{χ^2} that the data fit a model with α_s constant as a function of cms energy is smaller than 3%, whereas the probability for $\mathcal{O}(\alpha_s^3)$ running of α_s is larger than 50%. At larger values of $y_{\rm cut}$, the differences in probabilities between running and constant α_s become smaller. At $y_{\rm cut} = 0.04$ the probabilities are similar for the two.

6 Summary

We have analysed hadronic final states of e^+e^- annihilation events at LEP at cms energies of $\sqrt{s} = 91.2, 130 - -136, 161$ and 172 GeV in order to study the running of the strong coupling constant α_s. We compared the moments of the thrust and the C-parameter as well as the mean jet multiplicity $\langle N_{\rm jet} \rangle$ to QCD calculations.

For the moments of thrust and C-parameter, we show that the $\mathcal{O}(\alpha_s^2)$ predictions including power corrections for the first moments and with optimised values of the renormalisation scale parameter provide a good simultaneous description of the energy evolution of the first three moments. For higher moments, the power corrections become small and can safely be neglected at LEP1 and LEP2.

From separate fits of the first three moments to all energy points we find good agreement of the data with the QCD predictions with a running coupling α_s. The confidence limit for the exclusion of a constant α_s with $x_\mu = 1$ is at least 95% from the experimentally most sensitive fit to the first moment of C.

Fits of the mean jet multiplicity at all energy points at jet resolution values $y_{\rm cut} =$ 0.001, 0.005 and 0.04 result in a good description of the data. At the smallest value of $y_{\rm cut}$, the data exclude a model with α_s constant with a confidence limit of at least 95%, whereas the probability is large (around 50%) for a running α_s.

We thereby confirm the running of α_s, as predicted by QCD, between LEP1 and LEP2. With larger statistical precision in the forthcoming years of LEP2 this demonstration should become yet more significant.

References

[1] S. Bethke: Nucl. Phys. Proc. Suppl. A 54 (1997) 314

[2] M. Schmelling: In: ICHEP '96: Proceedings, Z. Ajduk and A. K. Wroblewski (eds.), World Scientific (1997)

[3] OPAL Coll., P. D. Acton et al.: Z. Phys. C 55 (1992) 1

[4] OPAL Coll., P. D. Acton et al.: Z. Phys. C 59 (1993) 1

[5] OPAL Coll., G. Alexander et al.: Z. Phys. C 72 (1996) 191

[6] OPAL Coll., K. Ackerstaff et al.: CERN-PPE/97-015, Acc. by Z. Phys. C

[7] OPAL Coll., K. Ackerstaff et al.: OPAL physics note PN 281 (1997), unpublished

[8] S. Catani et al.: Phys. Lett. B 269 (1991) 432

[9] R.K. Ellis, W.J. Stirling and B.R. Webber: QCD and Collider Physics. Vol. 8 of Cambridge Monographs on Particle Physics, Nuclear Physics and Cosmology, Cambridge University Press (1996)

[10] Z. Kunszt and P. Nason [conv.]: In: Z physics at LEP 1, G.Altarelli, R.Kleiss and C.Verzegnassi (eds.), Vol. 1, CERN 89-08 (1989)

[11] S. Catani and M.H. Seymour: Phys. Lett. B 378 (1996) 287

[12] Yu. L. Dokshitser and B.R. Webber: Phys. Lett. B 352 (1995) 451

[13] Mike Seymour: private communication

[14] T. Sjöstrand: Comput. Phys. Commun. 82 (1994) 74

[15] G. Marchesini et al.: Comput. Phys. Commun. 67 (1992) 465

[16] OPAL Coll., G. Alexander et al.: Z. Phys. C 69 (1996) 543

[17] S. Catani, Yu. L. Dokshitser, F. Fiorani and B.R. Webber: Nucl. Phys. B 377 (1992) 445

[18] OPAL Coll., K. Ahmet et al.: Nucl. Instrum. Methods A 305 (1991) 275

[19] OPAL Coll., G. Alexander et al.: Z. Phys. C 52 (1991) 175

[20] J. Allison et al.: Nucl. Instrum. Methods A 317 (1992) 47

[21] OPAL Coll., K. Ackerstaff et al.: Phys. Lett. B 389 (1996) 616

[22] J. Fujimoto et al.: Comput. Phys. Commun. 100 (1997) 128

[23] B.R. Webber: In: Workshop on Deep Inelastic Scattering and QCD, J.F. Laporte and Y. Sirois (eds.), Ecole Polytechnique (1995)

[24] H1 Coll., C. Adloff et al.: DESY 97-098 (1997), Sub. to Phys. Lett. B

[25] R. Barlow: MAN/HEP/93/9 (1993), Sub. to J. Phys. G

[26] V. A. Khoze and W. Ochs: MPI-Ph/96-29 and Durham DTP/96/36 (1996), Sub. to Int. J. Mod. Phys. A

Moment		JETSET 7.4		HERWIG 5.9	
		$\langle(1-T)^n\rangle$	$\langle C^n\rangle$	$\langle(1-T)^n\rangle$	$\langle C^n\rangle$
1	$\alpha_s(M_{Z^0})$	0.1081	0.1110	0.1074	0.1112
	$\bar{\alpha}_0$	0.380	0.314	0.435	0.336
	χ^2/d.o.f.	16	7.5	7.1	1.6
2	$\alpha_s(M_{Z^0})$	0.1121	0.1144	0.1151	0.1164
	$\bar{\alpha}_1$	1.34	1.65	1.62	1.7
	χ^2/d.o.f.	4.8	1.6	1.9	11
3	$\alpha_s(M_{Z^0})$	0.1131	0.1148	0.1183	0.1181
	$\bar{\alpha}_2$	5.7	25	6.8	23
	χ^2/d.o.f.	3.0	1.3	1.7	9.9

Table 1: Results of fits of $\mathcal{O}(\alpha_s^2)$ QCD with power corrections to the first three moments of the $1-T$ and C from the JETSET 7.4 and the HERWIG 5.9 Monte Carlo at the hadron level. The fits use $x_\mu = 0.05$ and $\mu_I = 2$ GeV. The precision of the numbers shown for $\alpha_s(M_{Z^0})$ and $\bar{\alpha}_n$ is to within the last digit shown.

	$1-T$	C
$\boldsymbol{\alpha_s(M_{Z^0})}$	**0.1271**	**0.1286**
$\alpha_s(M_{Z^0})$ (x_μ fitted)	0.1143	0.1158
x_μ	0.038	0.052
$\bar{\alpha}_0$	0.322	0.249
χ^2/d.o.f.	5.8/9	9.4/9
$\alpha_s(M_{Z^0})$ ($x_\mu = 1$)	0.1399	0.1414
stat. error	$\pm$0.0001	$<$0.0001
total exp. error	$\pm$0.0017	$\pm$0.0012
renorm. scale	$\pm$0.0074	$\pm$0.0074
$\mu_I \pm 1$ GeV	$\pm$0.0003	$\pm$0.0003
JETSET had. corr.	$-$0.0044	$-$0.0070
total theory error	$\pm$0.0087	$\pm$0.0102
total error	**$\pm$0.0088**	**$\pm$0.0102**

Table 2: Results for $\alpha_s(M_{Z^0})$ of simultaneous fits of $\mathcal{O}(\alpha_s^2)$ QCD to the first three moments of $1-T$ and C at the LEP1, LEP1.5 and LEP2 energy points. Power corrections are used only for the first moments of $1-T$ and C.

		$1-T$			C		
Moment		1	2	3	1	2	3
Power corrections							
$\mathcal{O}(\alpha_s^3)$ running	$\alpha_s(M_{Z^0})$	0.1146	0.1145	0.1144	0.1164	0.1164	0.1164
$\bar{\alpha}_0$ and x_μ	χ^2/d.o.f.	2.1/3	2.9/3	3.3/3	2.3/3	2.7/3	2.9/3
from sim. fit	P_{χ^2}	0.55	0.41	0.35	0.52	0.45	0.41
$\mathcal{O}(\alpha_s^3)$ running	$\alpha_s(M_{Z^0})$	0.1273	0.1533	0.1594	0.1307	0.1537	0.1609
$\bar{\alpha}_0$ from sim. fit	χ^2/d.o.f.	2.3/3	3.1/3	3.5/3	2.8/3	3.1/3	3.1/3
$x_\mu = 1$	P_{χ^2}	0.51	0.37	0.32	0.42	0.37	0.38
constant α_s	α_s	0.1272	0.1521	0.1549	0.1287	0.1518	0.1594
$\bar{\alpha}_0$ from sim. fit	χ^2/d.o.f.	8.5/3	6.5/3	5.6/3	14/3	11/3	7.2/3
$x_\mu = 1$	P_{χ^2}	0.037	0.092	0.13	0.0026	0.012	0.067
JETSET hadronisation corrections							
constant α_s	α_s	0.1254	0.1421	0.1492	0.1228	0.1403	0.1499
	χ^2/d.o.f.	6.8/3	4.8/3	4.7/3	8.4/3	6.2/3	4.9/3
$x_\mu = 1$	P_{χ^2}	0.078	0.19	0.20	0.039	0.10	0.18

Table 3: Results for α_s, χ^2/d.o.f. and the χ^2 probabilities P_{χ^2} from separate fits with running or constant α_s to each of the first three moments at all four energy points.

		$y_{\rm cut} = 0.001$	$y_{\rm cut} = 0.005$	$y_{\rm cut} = 0.04$	x_μ
$\mathcal{O}(\alpha_s^3)$ running					
R	$\alpha_s(M_{Z^0})$	0.1266 ± 0.0014	0.1267 ± 0.0023	0.1238 ± 0.0032	1.0
$\ln(R)$	$\alpha_s(M_{Z^0})$	0.1189 ± 0.0012	0.1208 ± 0.0020	0.1212 ± 0.0031	1.0
mod $\ln(R)$	$\alpha_s(M_{Z^0})$	0.1249 ± 0.0014	0.1259 ± 0.0023	0.1229 ± 0.0032	1.0
pure $\mathcal{O}(\alpha_s^2)$	$\alpha_s(M_{Z^0})$	-	-	0.1248 ± 0.0033	1.0
pure $\mathcal{O}(\alpha_s^2)$	$\alpha_s(M_{Z^0})$	-	-	0.1157 ± 0.0027	0.067
	χ^2/d.o.f.	2.3 / 3	2.0 / 3	1.2 / 3	
	P_{χ^2}	0.51	0.58	0.75	
constant α_s					
R	α_s	0.1242 ± 0.0014	0.1242 ± 0.0022	0.1229 ± 0.0032	1.0
	χ^2/d.o.f.	9.3 / 3	5.9 / 3	1.6 / 3	
	P_{χ^2}	0.026	0.12	0.65	

Table 4: Results for α_s using the mean jet multiplicity $\langle N_{\rm jet} \rangle$, at y_{cut} values of 0.001, 0.005 and 0.04. The fits are performed with $\mathcal{O}(\alpha_s^3)$ running of α_s (top part) and with α_s constant as a function of cms energy (lower part). The errors on α_s represent the total experimental uncertainties. Results for the χ^2/d.o.f. and the χ^2 probabilities P_{χ^2} are listed as well.

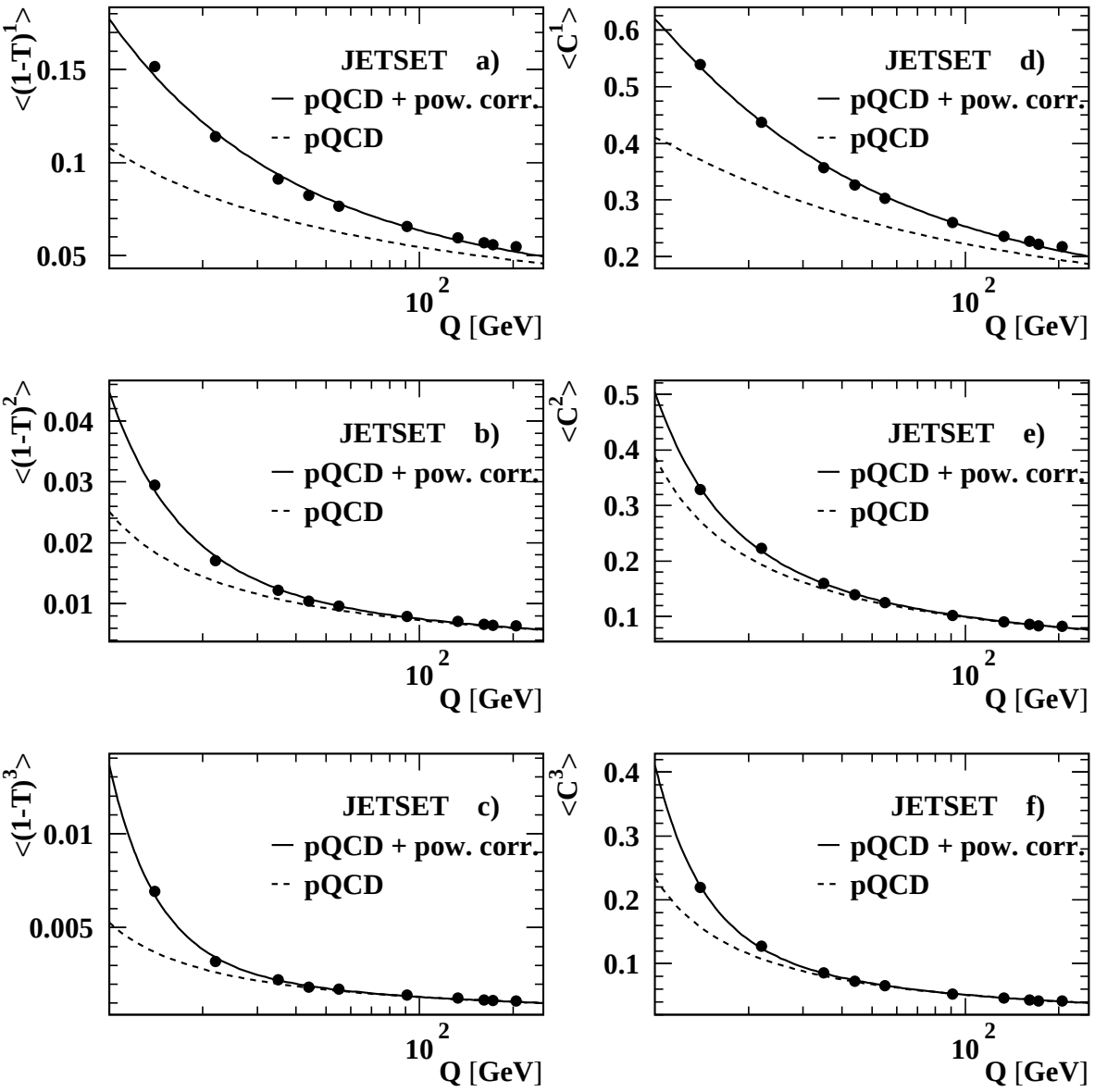

Figure 1: The energy evolution of the first three moments of the $1-T$ distribution (plots a) to c)) and the C distribution (plots d) to f)) predicted by the JETSET 7.4 Monte Carlo program at the hadron level. Superimposed are fits of the perturbative QCD prediction with power correction (full lines) and the purely perturbative part of the fit (dashed lines).

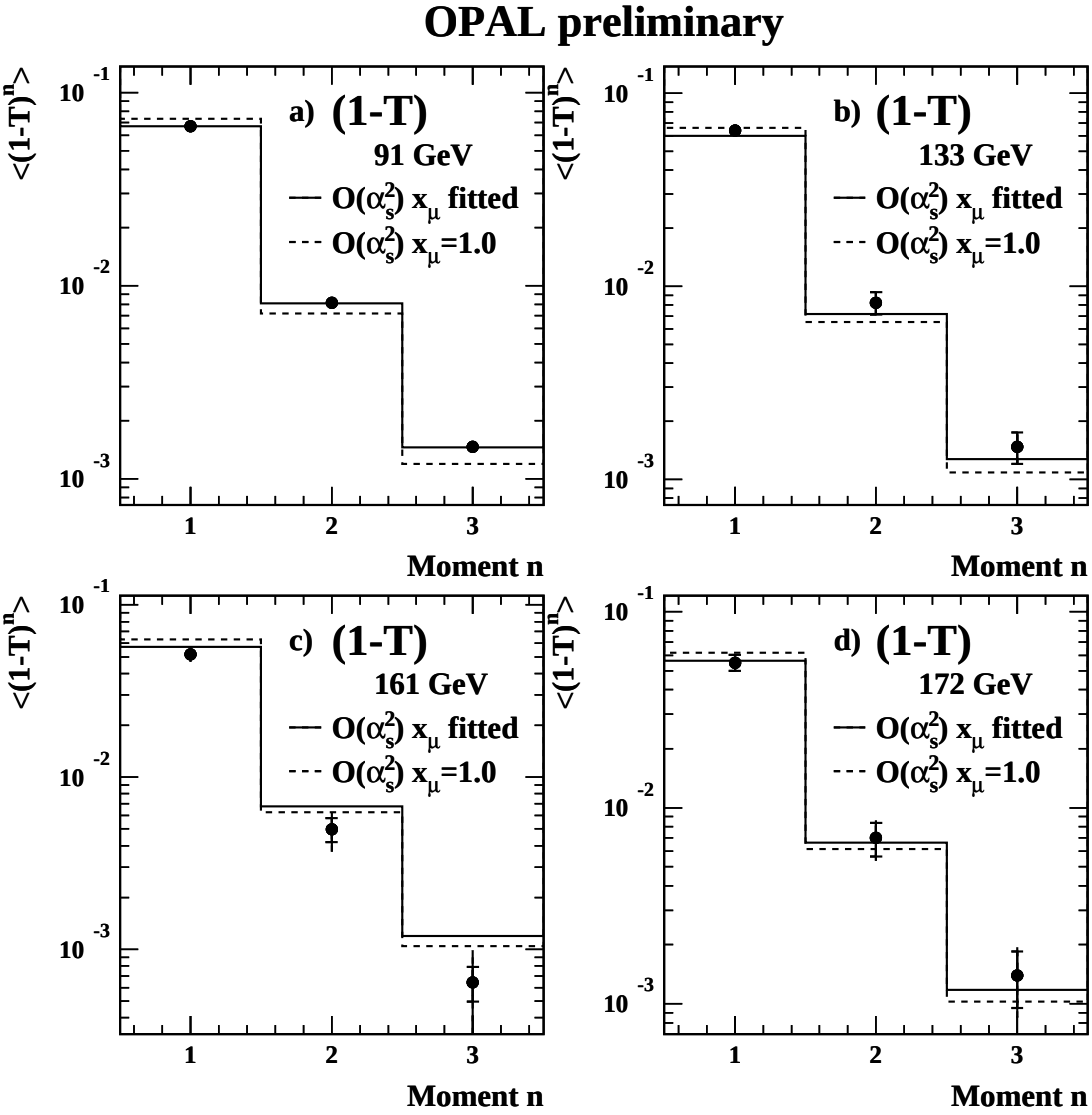

Figure 2: The points with error bars represent the data at the hadron level for the moments of $1-T$ at $\sqrt{s} = M_{\mathrm{Z^0}}$, 133, 161 and 172 GeV. The experimental uncertainties are shown by the full error bars while the statistical errors are indicated by the small horizontal lines. These are invisible in some cases. Superimposed is a fit of $\mathcal{O}(\alpha_s^2)$ QCD including the power correction for the first moment with the renormalisation scale parameter x_μ free (solid lines) and with $x_\mu = 1.0$ kept fixed (dashed lines).

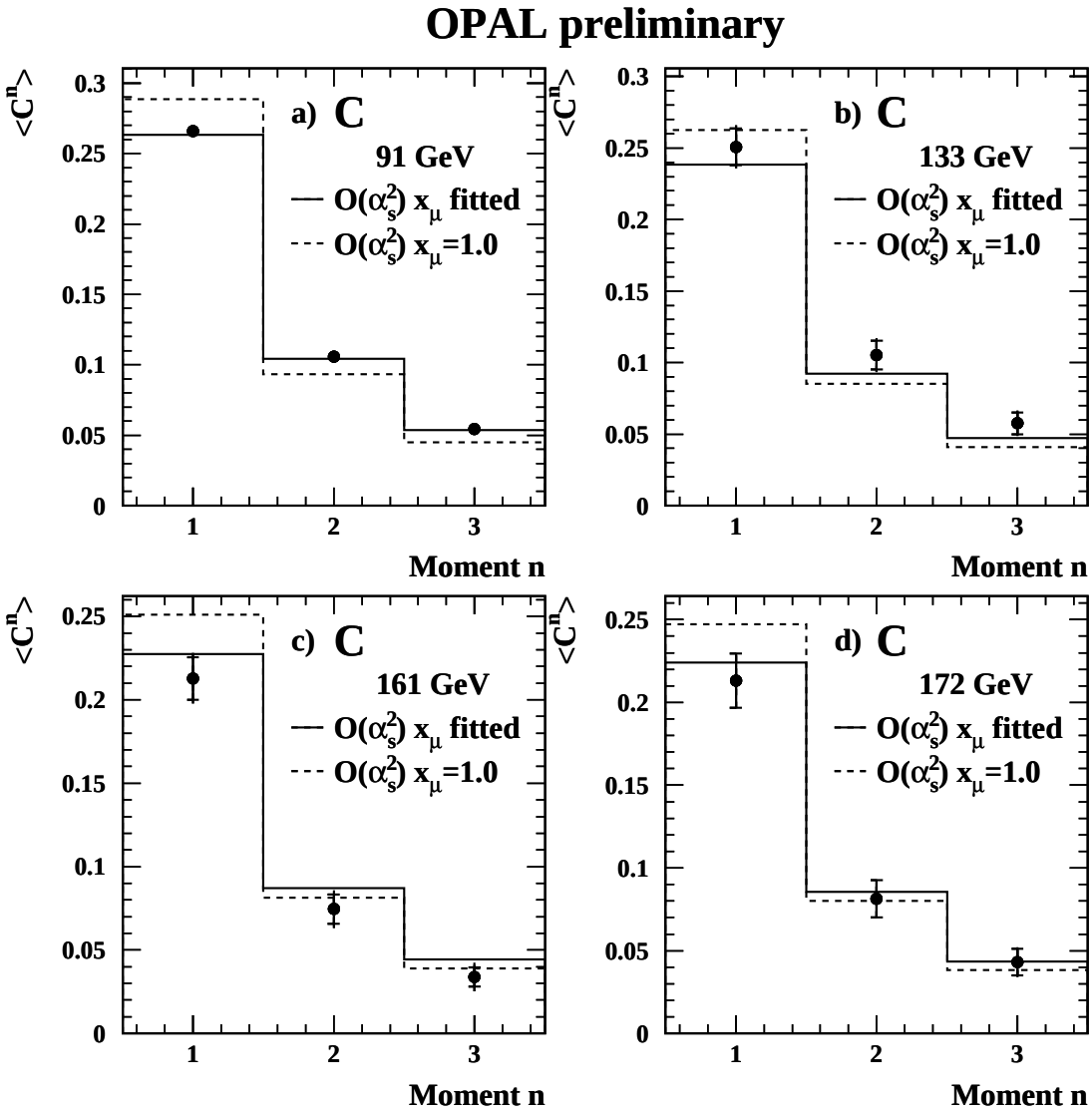

Figure 3: The points with error bars represent the data at the hadron level for the moments of C at $\sqrt{s} = M_{Z^0}$, 133, 161 and 172 GeV. The experimental uncertainties are shown by the full error bars while the statistical errors are indicated by the small horizontal lines. These are invisible in some cases. Superimposed is a fit of $\mathcal{O}(\alpha_s^2)$ QCD including the power correction for the first moment with the renormalisation scale parameter x_μ free (solid lines) and with $x_\mu = 1.0$ kept fixed (dashed lines).

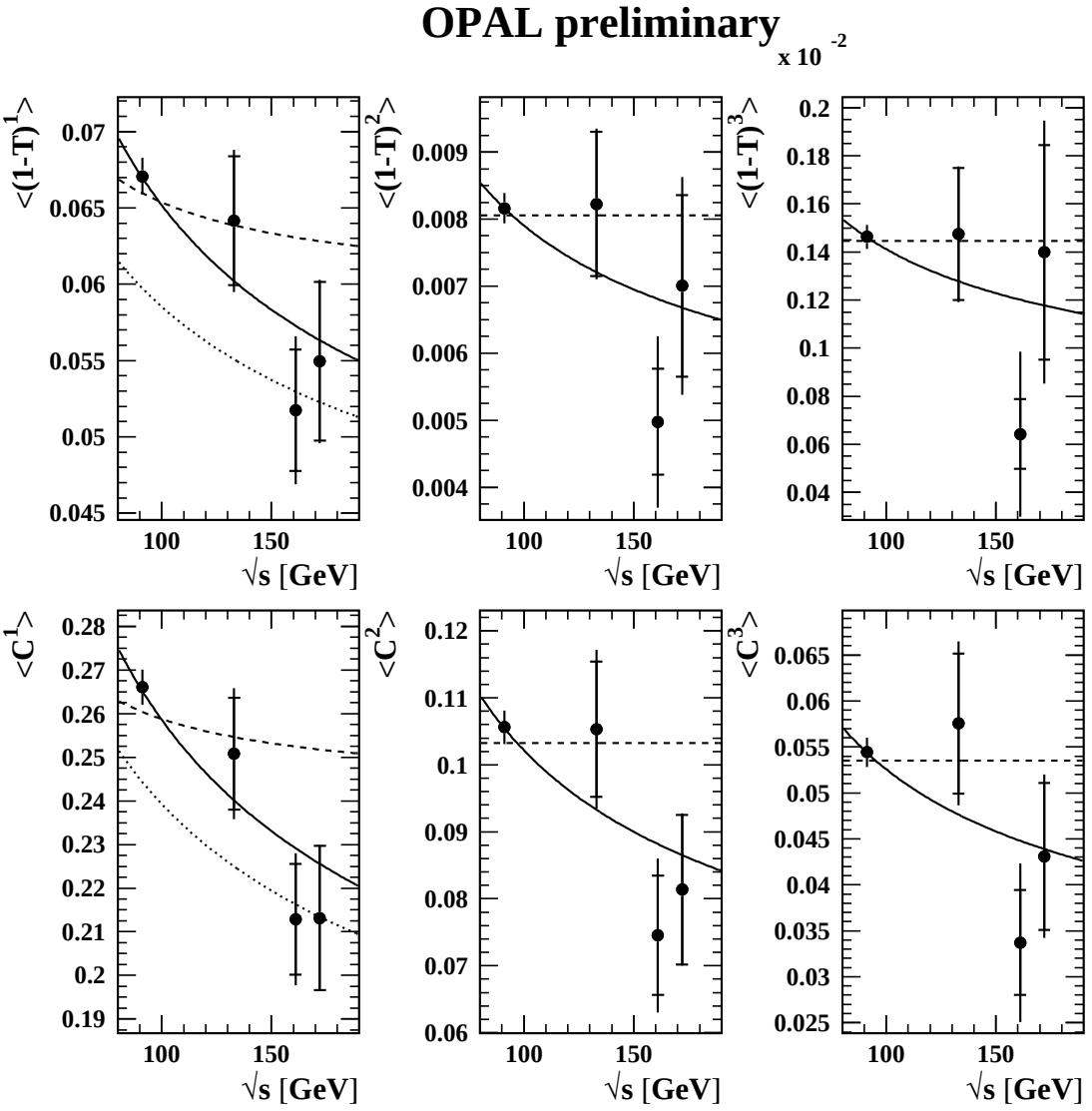

Figure 4: The points with error bars represent the data at the hadron level for the first three moments of $1-T$ and C at $\sqrt{s} = M_{\mathrm{Z^0}}$, 133, 161 and 172 GeV. The experimental uncertainties are shown by the full error bars while the statistical errors are indicated by the small horizontal lines. Superimposed are fits of $\mathcal{O}(\alpha_s^2)$ QCD including power corrections with a running α_s (solid lines) and with a constant α_s (dashed lines). The perturbative part for the fits to the first moments with a running α_s is shown by the dotted lines.

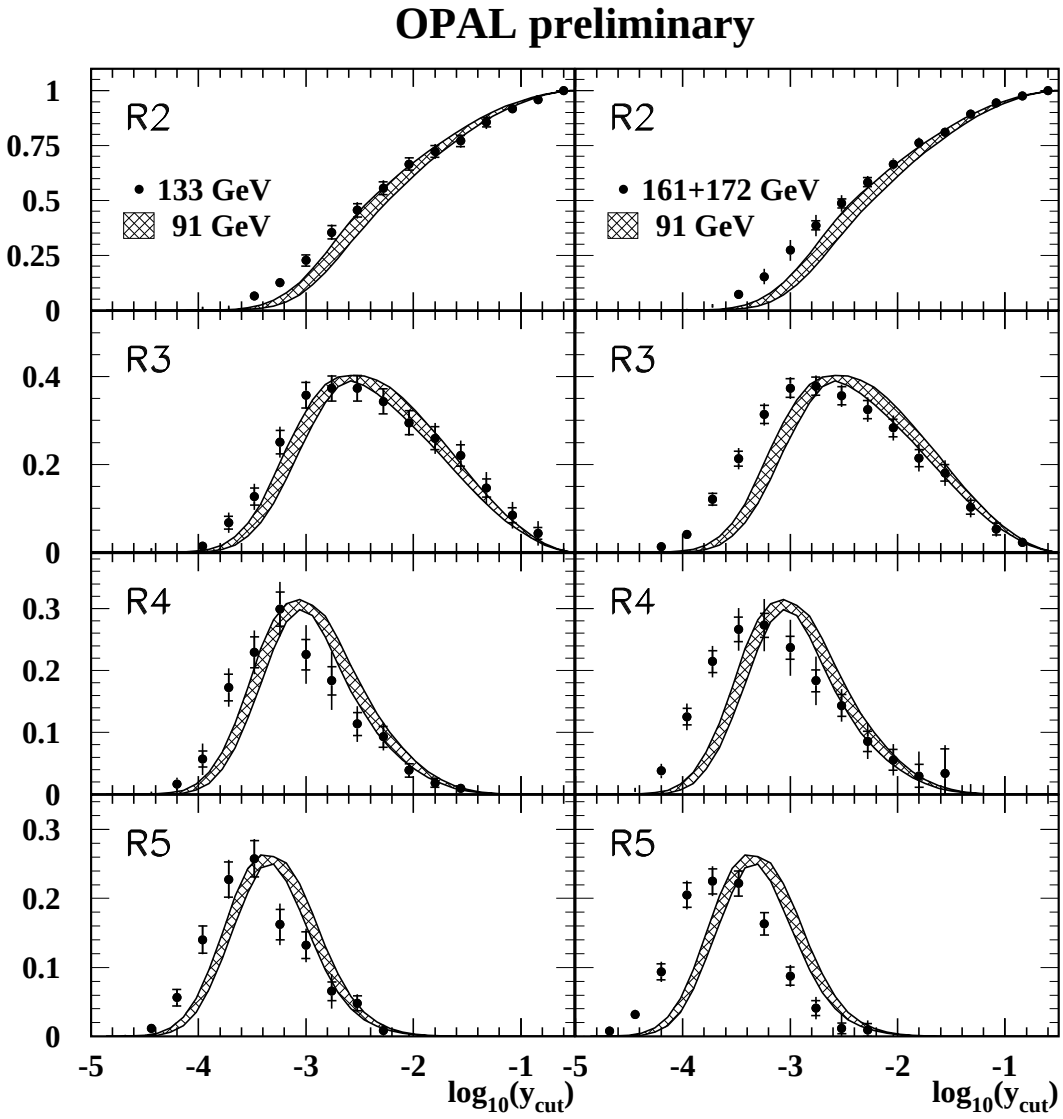

Figure 5: The jet production rates $R_{\rm n}(y_{\rm cut})$, for n from 2 to 5, for the Durham recombination scheme. The smooth histograms show the jet rates at $\sqrt{s} = M_{\rm Z^0}$, with the hatched band representing the systematic uncertainties. The points with error bars show the jet production rates at LEP1.5 (left column) and at LEP2 (right column) The experimental uncertainties are shown by the full error bars while the statistical errors are indicated by the small horizontal lines. The results at LEP2 are an average of the data from 161 and 172 GeV.

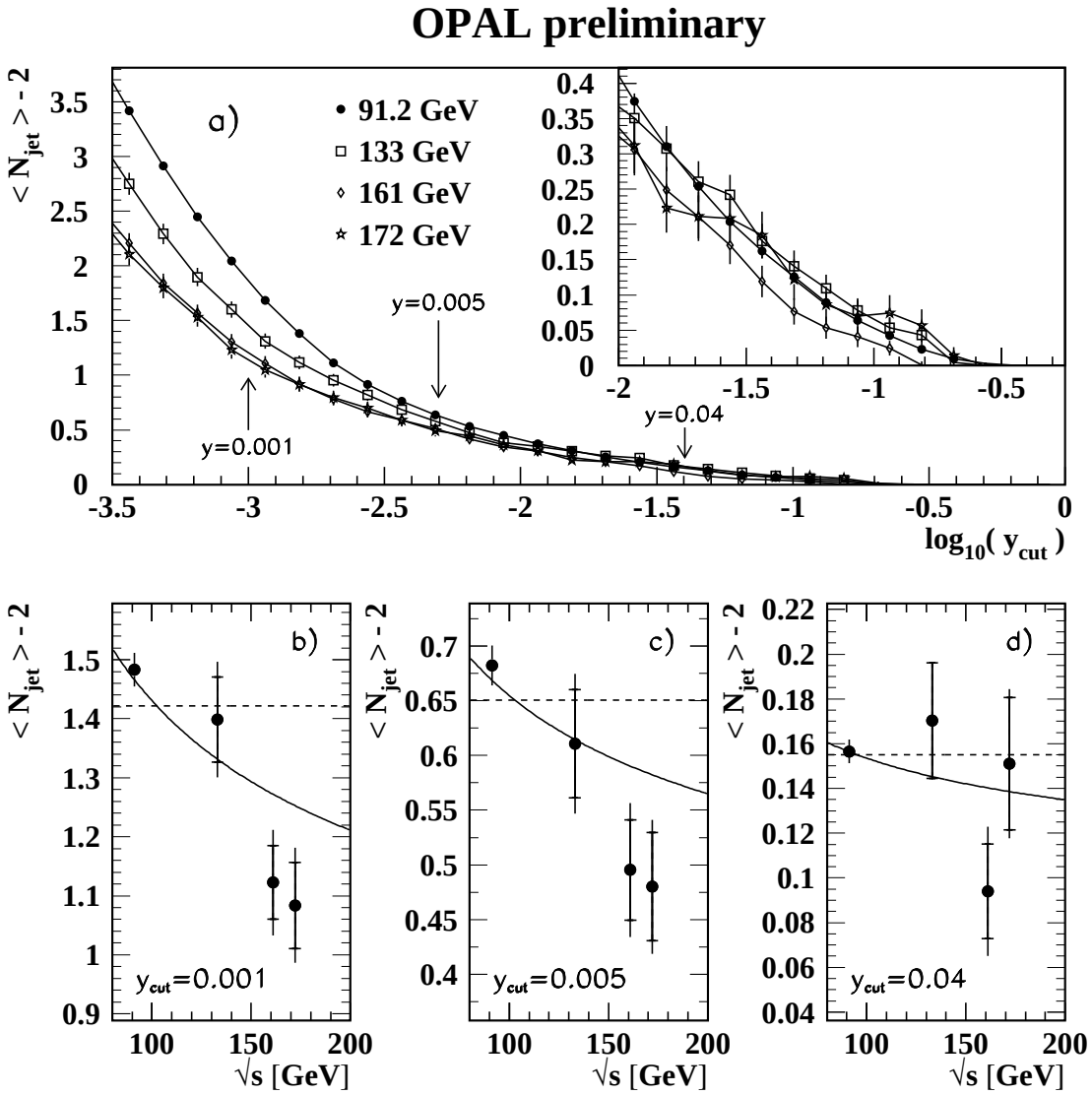

Figure 6: a) The mean jet rate $\langle N_{\rm jet}\rangle - 2$ at the hadron level, as a function of $y_{\rm cut}$. The inset shows the region for large values of $y_{\rm cut}$. The points corresponding to the same cms energy are connected by a line. b), c) and d) Fits to $\langle N_{\rm jet}\rangle - 2$ at fixed values of $y_{\rm cut}$ as indicated in the figure. The full line shows the fit with running of α_s, the dashed line for constant α_s. The data are corrected to the parton level. The experimental uncertainties are shown by the full error bars while the statistical errors are indicated by the small horizontal lines.